Scientific Research Publishing

Open Journal of Geology, 2025, 15(2), 87-108
https://www.scirp.org/journal/ojg
ISSN Online: 2161-7589
ISSN Print: 2161-7570

# Petrography and Geochemical Studies of Granitoids from Iro Lake South-East of Moyen Chari in Chad and Geodynamic Implication

**Leontine Tekoum[1,2*], Djatibeye Barnabe[2], Jean Claude Doumnang Mbaigane[1]**

[1]Laboratory of Geology, Geomorphology and Teledetection, Geology Department, Faculty of Exact and Applied Sciences, University of N'Djamena, N'Djaména, Chad
[2]Laboratory of Hydro-Geoscience and Reservoir, Geology Department, Faculty of Exact and Applied Sciences, University of N'Djamena, N'Djaména, Chad
Email: *leontinetekoum@yahoo.fr

**How to cite this paper:** Tekoum, L., Barnabe, D. and Mbaigane, J.C.D. (2025) Petrography and Geochemical Studies of Granitoids from Iro Lake South-East of Moyen Chari in Chad and Geodynamic Implication. *Open Journal of Geology*, **15**, 87-108.
https://doi.org/10.4236/ojg.2025.152004

**Received:** December 9, 2024
**Accepted:** February 25, 2025
**Published:** February 28, 2025



## Abstract

Located in Southeastern Chad. The Iro lake offers a great opportunity for the study of Precambrian formations and their Phanerozoic cover. Pluton is a Cal-alkaline granite. Due to its geographical location and geological features, it holds crucial information for understanding the evolution of the Saharan Meta craton (central Africa), which remains poorly studied. One of the objectives is to map the formations Precambrian age in Southeastern Chad. Based on the petrographic and geochemical results, we identified granitoids of pan-African age (biotite granite, aplite granite and pegmatite granite). This Precambrian basement is covered with sedimentary formations (clays, argillites, lateritic cuirasses, etc.). The mineral assemblage is characteristic of acid rocks. Geochemistry reveals rocks with a high $SiO_2$ range (62% - 77%) giving sub-alkaline to calc-alkaline acid rocks with high k (4.62% to 6.39%). The granitoids are classified as S-type hyperaluminous granites. This classification is supported by the presence of peraluminous minerals (e.g., muscovite) within the Iro granitoids, which also have high (>1%). Geochemical variation within the granites is largely due to extensive crystal fractionation. The Pattern of REEs normalized to the primitive mantle shows a pronounced negative Eu anomaly, reflecting the crystallization process and fractional crystallization of plagioclase in the rock, and a positive Yb anomaly. The role of plagioclase fractionation was relatively major during the earlier intrusive stages (consistent with the presence of Eu anomalies) and slightly increased, together with biotite and K-feldspar fractionation, during the later (granitic) rock crystallization. The Pattern of the spider normalized to MORBs shows two pronounced negative anomalies in $TiO_2$ and Cs and a slight negative anomaly in Ba. The loss of Ba,

Ti and Cs may be caused by the plagioclase fractionation, apatite and ilmenite crystal. The Ba anomaly is also controlled by the presence of K-feldspar and mica. The observed Ti anomalies are due to the fractionation of magnetite indicating a subduction environment (or remelting of a source from a subduction environment).

## Keywords

Petrography, Geochemical, Granitoids, Iro Lake, Moyen-Chari, Chad

## 1. Introduction

Granitic rocks are intensively studied because they form in a variety of tectonic settings and thus provide important clues to the growth and reworking of continental crust and to regional tectonics and geodynamic processes [1]-[3]. Most granites form by melting pre-existing continental crust, supplemented in many cases, by a contribution from the mantle, especially in continental arc systems [4] [5].

Highly fractionated granites (>73 wt.% $SiO_2$) commonly have petrographic and geochemical features similar to the haplogranite (near minimum-temperature melt). It is difficult to discriminate their magmatic sources, origin and petrogenesis [6]-[8]. [9] proposed an I- and S-type granite classification scheme that relates granites to source rock compositions and suggested that I-type granites are mainly metaluminous and are generally derived from meta-igneous source rocks, whereas S-type granites are strongly peraluminous and generated by the partial melting of metasedimentary source material. The granites of Iro Lake are dated between 580-575 Ma, less than 20 Ma after the peak of metamorphism linked to arc accretion-collision [10]. This demonstrates a rapid change in magma sources and geodynamic setting at the end of the Ediacaran in southern Chad [11].

*The geological formations have been the subject of limited study*; *however*, *existing research remains insufficient*. Thus, it is important, even urgent, to deepen scientific research on these geological formations very complex. The most important problem is to research the origin of the granitoids which crop out at the edges of this supposed meteoritic lake [12] from petrographic and geochemical studies. Recent work [11] during the GELT project included description of the geological environment of the lake, assessment of its putative impact crater origin [12], characterization of its sedimentary filling and determination of the hydrological and hydrogeological features of the area [13]. The geology of the S-SE region of Chad is relatively unknown due to its geographical isolation and the large extension of laterite and recent sediment cover [11]. Here, we present new petrographical and geochemical, data for the granitic rocks of these five plutons, and use these data to: 1) determine the nature of the sources for the S-type granites, 2) determine the genetic relationship between these granites, and 3) give our contribution to understanding of this geodynamic chain.

## 2. Location and Geological Setting of the Study Area

The department of Iro Lake is located in the South-East of Chad in the Moyen-Chari region as shown in Figure 1. The area of the Department of Lake Iro is 17,800 km$^2$ and that of Iro Lake is 455 km$^2$. The study area covers two villages, namely: Karou, which is located in the North-West of the lake, has coordinates N10˚12'/E19˚19' and Massadjanga, to the South of the lake, N10˚00'/E19˚23'.

Chad is part of the Pan-African Mobile Zone of Central Africa which extends from Hoggar in the North of Congo and from West to East from the West African craton to the mobile zone of East Africa [14].

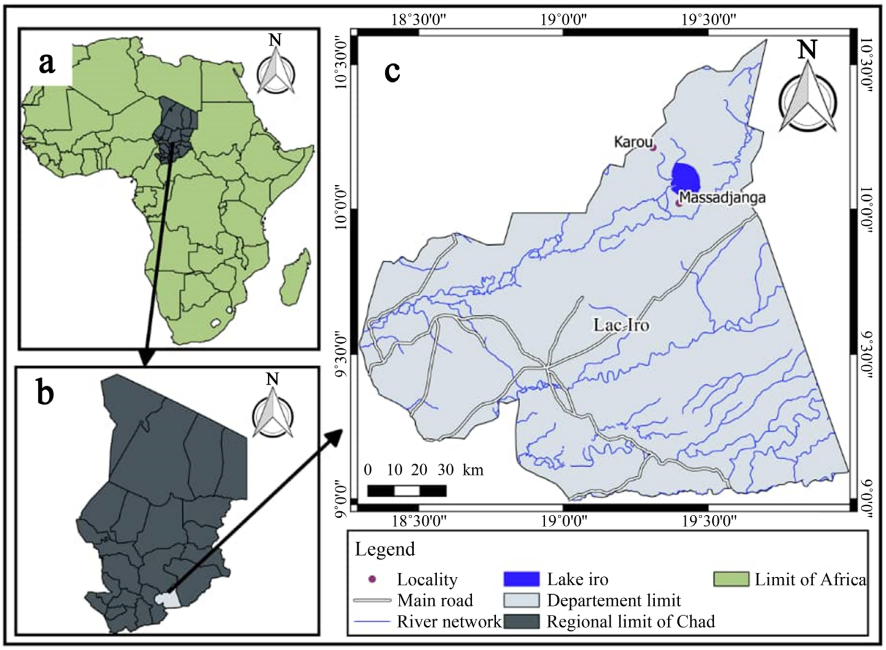


Figure 1. Map of the study area.

The knowledge of geology of Iro Lake region results from the collision between the Congo craton, the West African cratons and the hypothetical Nilotic blocks at Eastern Sahara between 900 and 550 Ma [15]-[20].

According to [14] [21] [22] the Chad region was tectonically stable after the Pan-African Orogeny, and sedimentary formations accumulated over most of its territory during the Palaeozoic. [23] conclude that magmatism was structurally controlled by Pan-African suture zones that were reactivated during the opening of the central Atlantic Ocean. In large lines, the Chadian subsoil is made up of crystalline rocks formed and/or influenced by Pan-African orogeny (Precambrian Basement). This basement was formed during the Pan-African orogeny that took place towards the end of the Precambrian (700 - 550 Ma) [24] [25]. This pan-African event represents the last active orogeny in Chad [26], [27]. The rocks formed are influenced by this event and make up the bulk of the crystalline massifs found in the Tibesti in the north, the Ouaddaï in the east, the Guera in the centre, the Mayo-Kebbi in the south-west and Baibokoum in the south [5] [26]. Previous work carried out in

the region focuses on rec pedological and hydrogeological research and a very first pioneering work on geology. Two large geological units stand out in the Iro Lake department: the rocky points of the base, the armors and the ancient sedimentary [28]. According to [11] the Lake Iro granites thus represent the oldest of a series of post-collisional igneous associations exposed in southern Chad and nearby countries which, collectively, show that the amalgamation of the constituent blocks of the southern Saharan Metacraton is older than 580 Ma.

In the west center of this department, the rocky points form real small massifs: Bon, Zan and Goumé. Elsewhere, the distribution is more heterogeneous, it ranges from true pointing to simple outcropping. From North to South, we will also cite a few more important points: Toumoudi, Adja, Ibir, Aya, Karou, and Massadjanga as shown in **Figure 2**. These granites are generally calc-alkaline. The young granites of Bombouri, on the edge of the western map of Iro Lake, represent the most alkaline of the central massif in Chad. The massifs or rocky points appear in the form of inselbergs or in piles [28].

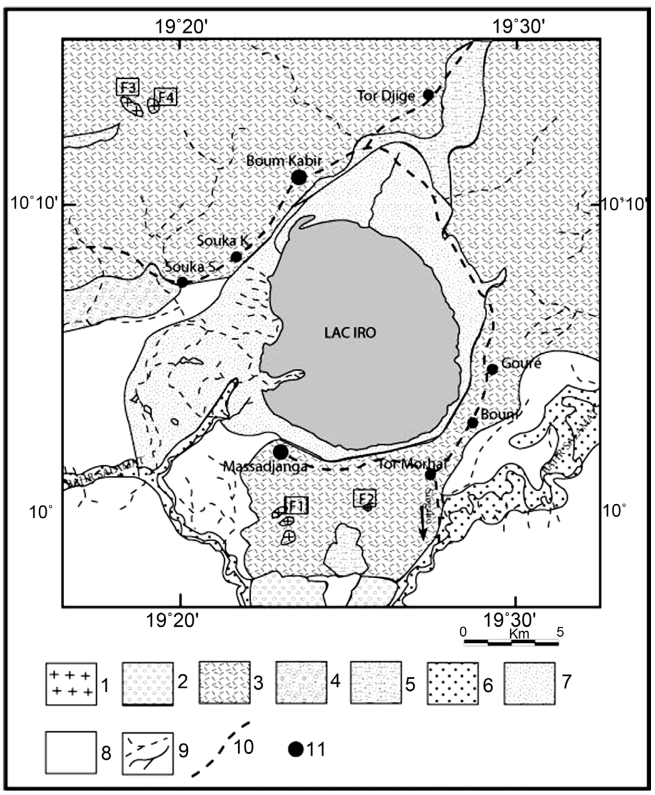


1: Granit; 2: Lateritic Cuirass; 3: Clayey-sandy material with limestone nodules; 4: Sandy-clay material; 5: Hydromorphic vertisol; 6: Clayey-silty alluvium; 7: Clay-sandy to clayey material; 8: Recent alluvium on clayey-sandy material; 9: Watercourses; 10: Roads; 11: Villages.

**Figure 2.** Geological Map of the study area after [29].

## 3. Material and Methods

The material includes field data (samples), laboratory data and satellite images

(Image 1, Image 2) were used. The first phase consisted of the collection of field data, through sampling of granitoids, samples were selected based on their geographical distribution within the pluton (Figure 3) in Massadjaga and Karou areas. The difficulty assessing the area during field work is due to the geographical isolation and the large extension of laterite. The preparation of twelve (12) thin sections at the Module Roche in the Laboratory of CEREGE, Aix En Provence (France) made it possible to determine the petrographic characteristics of granitoids. Geochemical analyses were carried out by the ICP-ES (Inductively Coupled Plasma-Emission Spectrometry) for the major elements and some minor elements and by the method ICP-MS (Inductively Coupled Plasma-mas Spectrometry), for trace elements and minors, at the CRPG (Petrographic and Geochemical Research Center) in Nancy/France.

The main advantage of ICP-MS is its analytical capacity, its speed (7 minutes/sample for 40 elements), its precision is one part per trillion (1 ppt = 10 - 12 g/g) and measurements of concentrations of trace elements with an error of 10% to 15% [29]. Also made it possible to clarify the petrographic nature, and environments of the establishment of these granitoids.

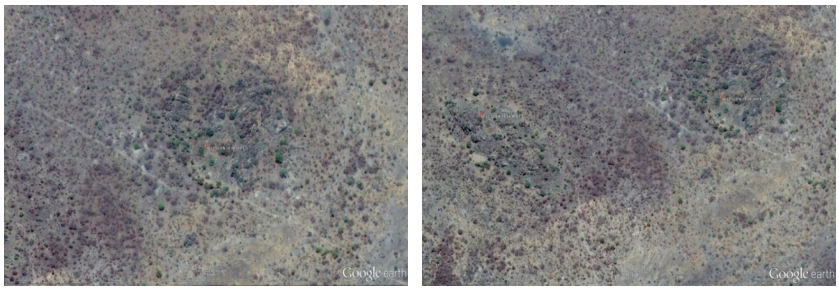

Image 1. Satellite image of Karou (Source Google Earth).

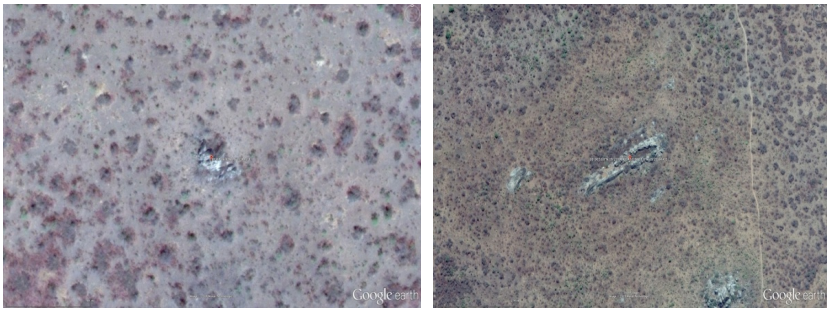

Image 2. Satellite image of Massadjanga (Source Google Earth).

## 4. Results

Field relationship and petrography

The plutonic formations that constitute the rocks of the study area are granitoids as shown in Figure 3. Coarse-grained granites, fine-grained granites and aplites outcrop in the form of granitic chaos, ball granites and slab granites. These different granite outcrops give fine-grained and coarse-grained granite types con-

taining dominant minerals such as quartz, feldspar, orthoclase, and biotite as well as fractures. From a petrographic point of view, the facies differ from each other ranging from very fine grains (aplite) to coarse grains (porphyries) and biotite granites. The field campaigns made it possible to observe: granites, aplites and pegmatites. According to the objectives set, granites are described in more detail than aplites and pegmatites.

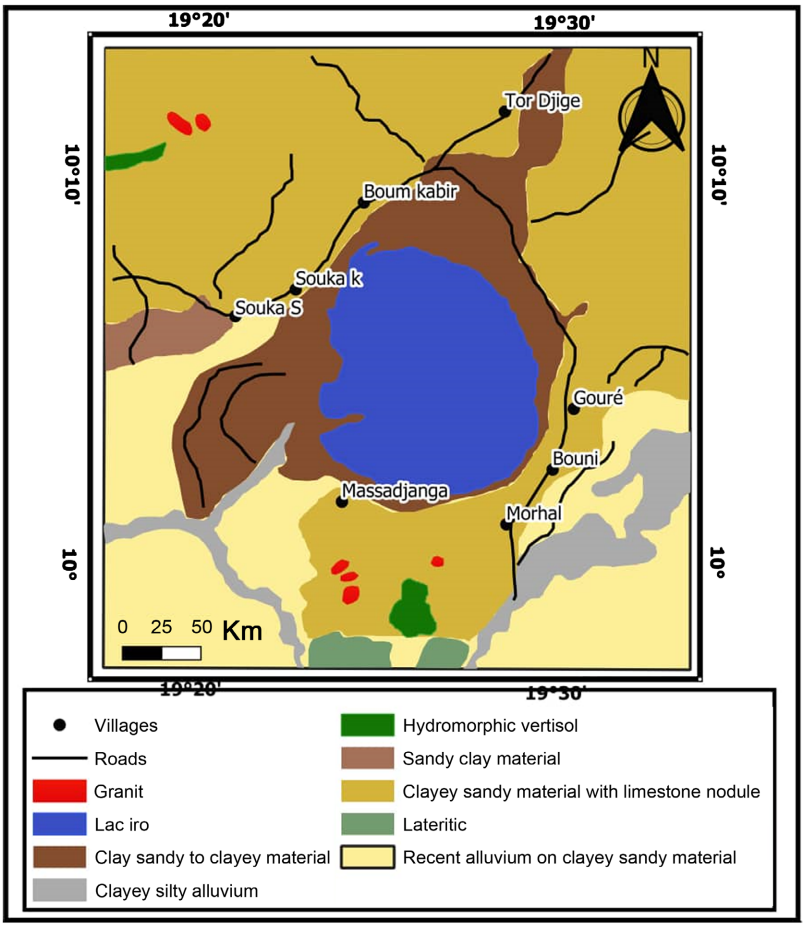


**Figure 3.** Map of sampling.

## 4.1. Petrographic Characteristic of Granites

### 4.1.1. Fine-Grained Granite

Macroscopic description

The fine-grained granite outcrop has the geographical coordinates N10˚00, E19˚23 with an altitude of 831 m south of Lake Iro (Massadjanga village). The structure is micro-grained to fine-grained but has two facies. Sample 16IRO 02. The dominant minerals are: quartz, biotite, orthoclase and feldspar. Structurally the directions observed on the fractures are N53˚ 85NW and N60˚ 85NW (**Figure 4(a)**).

Microscopic description Fine-grained granite has a microgranular texture. Mineralogically, the rock is composed of quartz, plagioclase, alkali feldspar, and biotite (**Figure 4(b)**) and is also composed of accessory minerals such as zircon, sphene and oxides. Alkali feldspars (35% - 45%) Alkali feldspars are composed of

microcline and orthoclase. Microcline is easily identified by the pericline twin on its edges while orthoclase, in elongated sections, is recognized by the Carlsbad twin. Orthoclase also occurs in the form of automorphic to subautomorphic areas of approximately a few millimeters in size containing opaque inclusions. Quartz (20% - 25%) occurs in the form of subautomorphic to xenomorphic crystals of medium size. Some quartz crystals are in interstitial form but others occur as quartz aggregates most often found on the edge of feldspars. Plagioclase (15% - 20%) is automorphic to subautomorphic, colorless and cloudy in appearance due to the phenomenon of alteration. Plagioclase crystals have Carlsbad twins. Their size is medium containing opaque inclusions. Biotite (5% - 10%) occurs in the form of flakes with a fine and regular cleavage. The color of biotite is yellowish-brown. Biotite has a size that varies between 0.15 to 0.30 mm and has inclusions of opaque minerals, apatite and zircon as well as some biotite flakes that alter into chlorite.

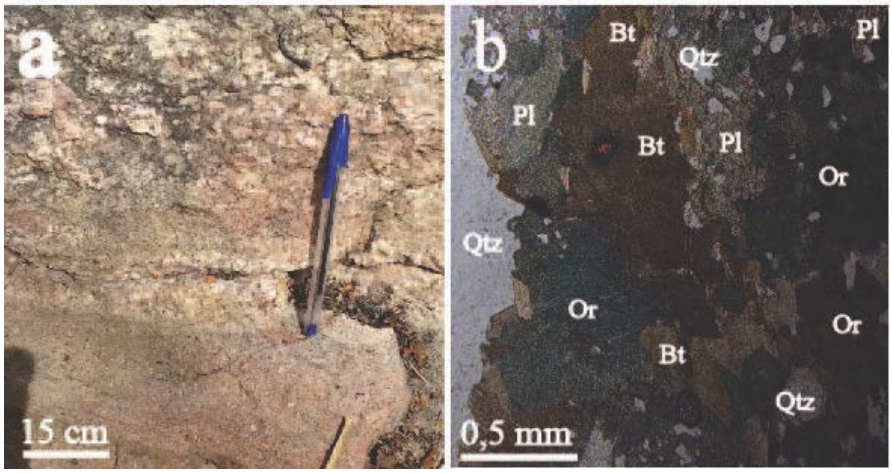


**Figure 4.** (a) Microgranite pink, (b) Microgranite-dominated thin portion. Qtz: quartz; pl: plagioclase; Or: orthose; Bt: biotite.

### 4.1.2. Coarse-Grained Granites

Macroscopic description at the outcrop, coarse-grained granites occur in the form of balls, slabs and granitic chaos to the NW of Lac Iro (Karou village) with coordinates N10˚12, E19˚19. It should be remembered that these rocks contain basic enclaves, quartz veins and pegmatites in places (**Figure 5(a)**). They are yellowish-gray in color and sometimes altered with a grainy texture whose observable mineral size is greater than 5 mm. Coarse-grained granites are composed in particular of quartz, alkali feldspar, plagioclase and biotite (**Figure 5(b)**).

Microscopic description Coarse-grained granites have a grainy texture. They are composed mainly of plagioclase, quartz, alkali feldspar, biotite, sphene; opaque, and apatite.

Plagioclase (25% - 30%) Plagioclase is Carlsbad twinned, polysynthetic and of low relief. This mineral shows overall subautomorphic to xenomorphic crystals of size varying between 0.1 mm to 0.5 mm. It occurs in the form of elongated areas showing inclusions of apatite and opaque.

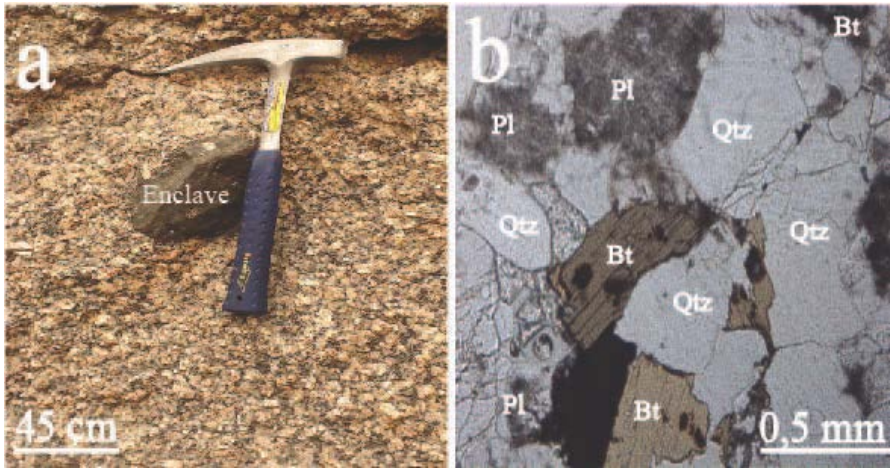


**Figure 5.** (a) Granite with circular enclave, (b) Portion of thin blade with granular texture dominated by quartz. Qtz: quartz; pl: plagioclase; Bt: biotite.

Quartz (20% - 25%) occurs as xenomorphic crystals slightly larger than plagioclase. Some are found as fine quartz grains in the interstices of orthoclase, plagioclase and biotite sections. Alkali feldspar (10% - 20%) identified is orthoclase. Orthoclase occurs as medium-sized, automorphic to subautomorphic crystals. It is Carlsbad twinned and cloudy in appearance. Some crystals are perthitic and show cracks filled with fine quartz grains but apatite and opaques are found as inclusions. Biotite (15% - 10%) occurs as medium-sized, yellowish-brown flakes. Cleavages are fine and regular. Opaque minerals are arranged along the cleavages. Biotite contains zircon as inclusion and alters to chlorite. Apatite occurs as clear elongated sections or as medium-sized stocky sections. It occurs as inclusion in alkali feldspar, plagioclase and biotite crystals.

Opaque minerals appear as brown-colored automorphic crystals abundant in the rock. These crystals are inclusions in plagioclase, feldspar and biotite crystals.

#### 4.1.3. Biotite Granite

Macroscopic description. Biotite granites are described in the village of Karou located in the NW of the lake, N10˚12/E19˚19 and in Massadjanga located in the South of the lake, N10˚00/E19˚23. They outcrop in slabs, granitic chaos and metric to decametric balls, but generally in the form of large massifs dominating the edges of Lake Iro. These are rocks with a grainy to micrograined texture, sometimes with a porphyritic tendency. They are generally composed of plagioclase, alkali feldspars, quartz, and biotite. At the outcrop, these granites have a gray to brown color with a dark gray weathering patina and are crossed by quartz-feldspathic veins. Aplites are also highlighted in these biotite granites (**Figure 6(a)**).

Microscopic description. The texture of biotite granites is granular to microgranular porphyritic with jointed crystals. They have plagioclase phenocrysts of size that varies between 0.03 mm and 1.5 mm. Their mineralogical composition

is mainly quartz, plagioclase, alkali feldspar, biotite and muscovite (Figure 6(b)). Accessory minerals are opaque, sphene and apatite as well as secondary minerals such as chlorite.

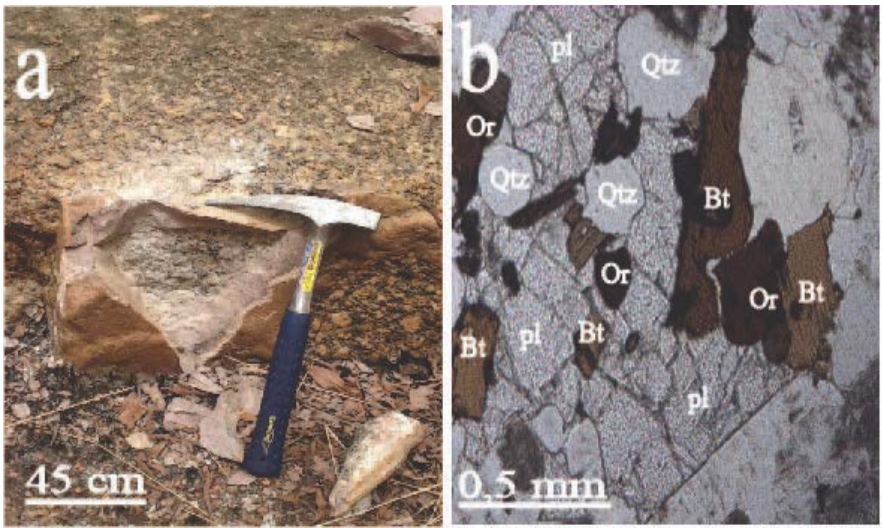


Figure 6. (a) Biotite granite from NW of Lake Iro, (b) Portion of thin section of coarse-grained texture of biotite granite. Qtz: quartz; pl: plagioclase; Or: orthose; Bt: biotite.

Alkali feldspars (35% - 45%) are essentially composed of microcline and orthoclase, the orthoclase of which is in automorphic to xenomorphic sections of varying size with Carlsbad twins. Quartz (25% - 30%) is in the form of xenomorphic crystals. The crystals are of medium size. It sometimes occurs in aggregates of contiguous crystals arranged in the interstices left by the alkali feldspar and plagioclase.

Biotite (10% - 15%) occurs in subautomorphic flakes, striated by very fine and regular cleavage with an average size and yellowish-brown color. The biotite sections are oriented in the rock. It is in inclusions in the large crystals of alkali feldspars. Biotite is destabilized and altered into chlorite. Plagioclase (5% - 10%) occurs in the form of large, medium-sized, automorphic to subautomorphic crystals. It presents the twinning of polysynthetic albite. Some crystals have quartz grains in contact with alkali feldspar. Plagioclase contains opaque inclusions and alters into epidote. Sphene is in small, corroded diamond-shaped sections. It is attached to biotite flakes. Apatite occurs in the form of small rods scattered abundantly in the rock. Opaque minerals appear in the form of automorphic to xenomorphic dark brown.

### 4.2. Geochemical Characteristics of Granites

Geochemical study of the main granitoids with the aim of comparing to groups of known rocks. Representative rock samples were analyzed (major elements, traces and rare earths) at the Petrographic Research Center and Geochemical (CRPG) of Nancy/France. In total, 12 samples of granitoids including 06 to Mas-

sadjanga (Iro 04, Iro 08, Iro 09, Iro 15, Iro 17 and Iro 18) and 06 in Karou (A1, A2, A3, A4, A5 and A6) with respectively a Loss on Fire (PF) of 0.6% to 0.5% were analyzed (Table 1).

**Table 1.** Chemical composition in major elements (% by weight) of representative samples of granite of Iro Lake.

| | A1 | A2 | A3 | A4 | A5 | A6 | Iro 04 | Iro 08 | Iro 09 | Iro 15 | Iro 17 | Iro 18 |
|---|---|---|---|---|---|---|---|---|---|---|---|---|
| | % | % | % | % | % | % | % | % | % | % | % | % |
| $SiO_2$ | 74.72 | 68.92 | 68.38 | 74.74 | 77.04 | 74.18 | 69.55 | 68.47 | 61.90 | 68.53 | 75.35 | 71.92 |
| $TiO_2$ | 0.14 | 0.66 | 0.76 | 0.14 | 0.09 | 0.15 | 0.64 | 0.54 | 1.49 | 0.38 | 0.05 | 0.09 |
| $Al_2O_3$ | 13.02 | 13.23 | 13.04 | 12.82 | 12.68 | 12.77 | 13.55 | 14.56 | 12.95 | 15.09 | 13.45 | 14.48 |
| $Fe_2O_3$ | 2.07 | 4.93 | 5.66 | 1.85 | 1.00 | 2.26 | 4.86 | 4.09 | 9.44 | 3.64 | 0.77 | 1.06 |
| MnO | 0.04 | 0.07 | 0.08 | 0.03 | 0.02 | 0.04 | 0.08 | 0.06 | 0.16 | 0.07 | <L.D. | 0.02 |
| MgO | 0.10 | 0.55 | 0.65 | 0.10 | 0.07 | 0.07 | 0.53 | 0.44 | 1.62 | 0.52 | 0.03 | 0.09 |
| CaO | 0.88 | 1.91 | 2.18 | 0.68 | 0.83 | 0.83 | 1.91 | 1.27 | 3.52 | 1.97 | 0.71 | 1.16 |
| $Na_2O$ | 3.30 | 3.09 | 3.12 | 3.11 | 3.07 | 3.25 | 3.16 | 3.16 | 2.76 | 3.76 | 3.83 | 3.40 |
| $K_2O$ | 5.35 | 5.27 | 4.92 | 5.42 | 5.20 | 5.31 | 5.48 | 6.39 | 4.63 | 5.67 | 5.72 | 6.11 |
| $P_2O_5$ | <L.D. | 0.23 | 0.32 | <L.D. | <L.D. | <L.D. | 0.23 | 0.23 | 0.64 | 0.14 | <L.D. | <L.D. |
| LOI | 0.78 | 0.72 | 0.65 | 1.10 | 0.29 | 0.75 | 0.62 | 1.00 | 0.97 | 0.66 | 0.73 | 0.71 |
| Sum | 100.40 | 99.61 | 99.75 | 99.99 | 100.29 | 99.60 | 100.59 | 100.20 | 100.07 | 100.41 | 100.65 | 99.03 |

The $Na_2O + K_2O$ vs $SiO_2$ diagram of [30] adapted to plutonic rocks (Figure 7) reveals at first glance that all granitoids are acidic with one exception (one sample falls in the Intermediate domain) and that they are located in the field of sub-alkaline rocks: these are subalkaline acid rocks.

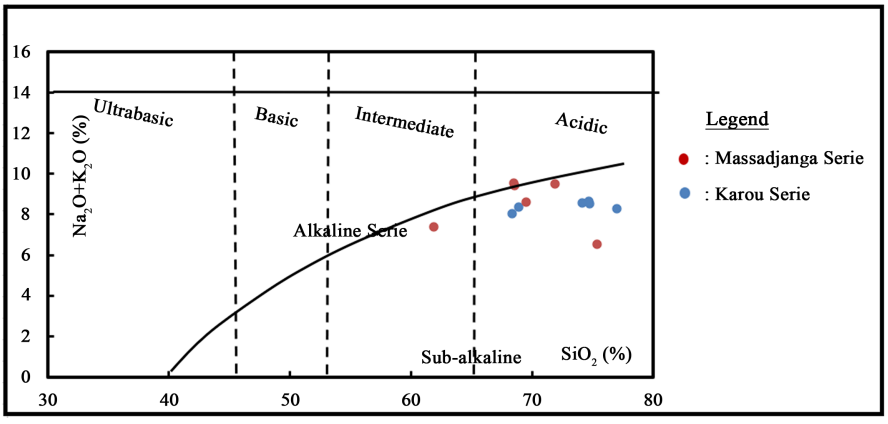


**Figure 7.** The Massadjanga and Karou granites, in the $Na_2O + K_2O$ vs $SiO_2$ diagram. The straight line limiting the fields of alkaline and sub-alkaline rocks is from Irvine and Baragar (1971).

In the $K_2O$ vs $SiO_2$ diagram (Figure 8). All samples have behavior of high K and plot to the cal-alkaline field characteristic of the subduction zone.

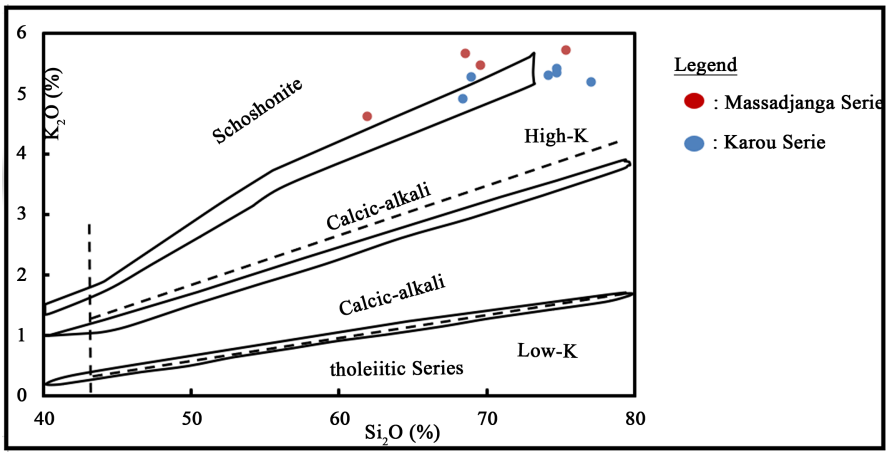


Figure 8. $K_2O$ vs $SiO_2$ diagram from [31] applied to the Karou and Massadjanga granites. The ligne limits are from [31] and the bands are from [32].

In the A/CNK (mol.) vs $SiO_2$ diagram, the Karou and Massadjanga granites with an A/CNK ratio > 1 are hyperaluminous (Figure 9). These granitoids are of type S, i.e. they are derived from magma originating from the fusion of igneous rocks [33].

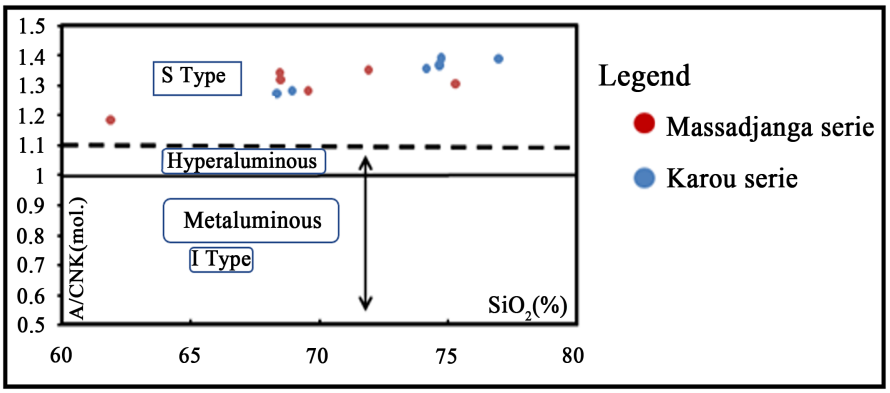


Figure 9. Projections of the Massadjanga granites and the Karou granites in the A/CNK (mol.) vs $SiO_2$ (%), diagram (A/CNK = $Al_2O_3$/(CaO + $Na_2O$ + $K_2O$) with A = $Al_2O_3$; C = CaO; N = $Na_2O$ and K = $K_2O$ [33].

### 4.2.1. Major Elements Analysis

Massadjanga granites

Chemical analysis shows that the Massadjanga granites show a high content of $SiO_2$ (75.35%), $Al_2O_3$ (15.09%), $Fe_2O_3$ (9.44%), $K_2O$ (6.39%), $Na_2O$ (3.83%), CaO (3.52%), MgO (1.62%) and $TiO_2$ (1.49%) but they have a low content of MnO (0.16%) and $P_2O_5$ (0.64%).

Karou granites

The Karou granites have a high content of $SiO_2$ (77.04%), $Al_2O_3$ (13.23%), $Fe_2O_3$

(5.66%), $K_2O$ (5.35%), $Na_2O$ (3.30%), CaO (2.18%) but a low MnO content (0.08%), MgO (0.65%), $TiO_2$ (0.76%) and $P_2O_5$ (0.32%).

The high contents of $SiO_2$ and alkaline ($Na_2O + K_2O$ = 6.55% - 9.55%) show a significant fractionation of plagioclase and alkali feldspar. $Fe_2O_3$, MgO and $TiO_2$ fractionate in biotite, $TiO_2$ and CaO fractionate in apatite $P_2O_5$ and $Fe_2O_3$ fractionate in opaque minerals as well.

Hacker diagrams $Al_2O_3$, CaO, MnO, $Na_2O$, $K_2O$ vs $SiO_2$ identify two groups of rocks: the group of Massadjanga microgranites and Karou granites. The $P_2O_5$, $TiO_2$ and MgO diagrams show a single group of rocks composed of microgranites from Massadjanga and granites from Karou. The only $Fe_2O_3$ diagram shows also a group made up of Massadjanga granites and Karou granites with a tendency negative development. The set of diagrams defines a negative trend as shown in Figure 10.

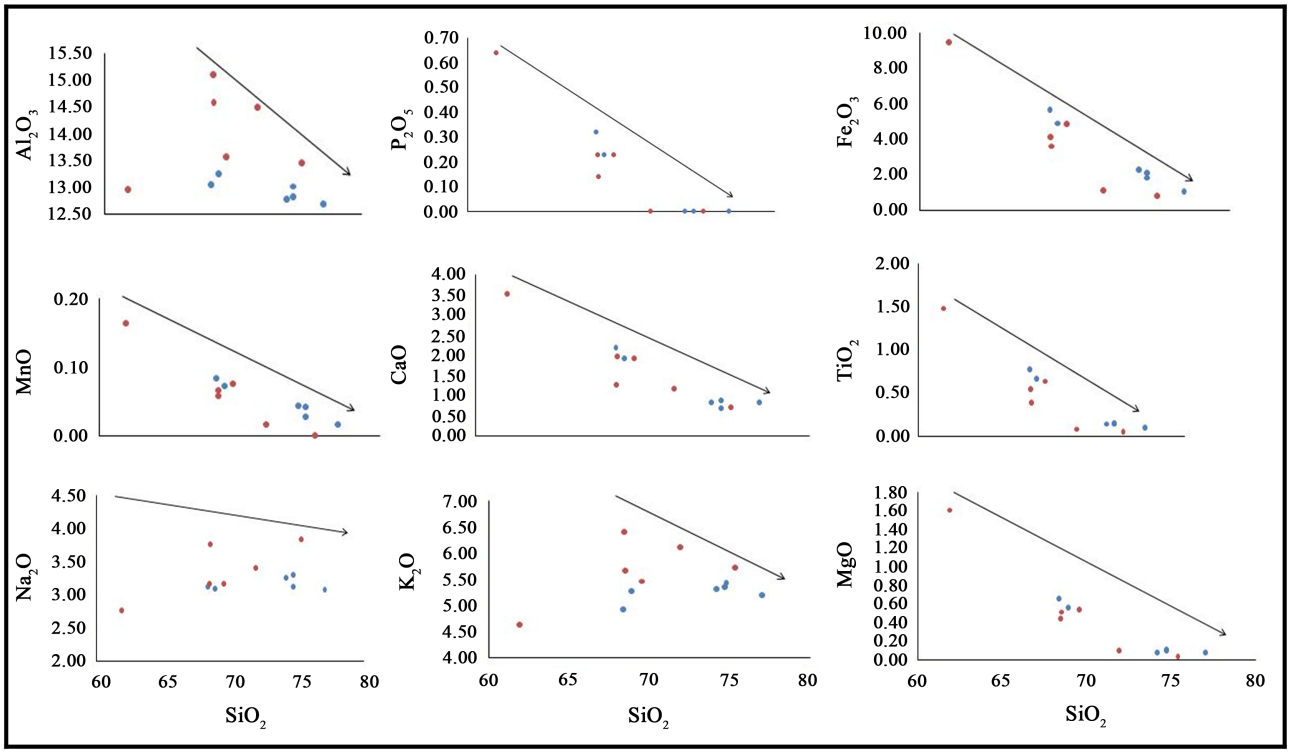


Figure 10. Hacker diagram showing the evolution of major elements as a function of $SiO_2$. The solid blue circle denotes the Massadjanga granites and the solid red circle denotes the Karou granites.

### 4.2.2. Trace Elements Variation

The description of trace elements takes into account Zr, Y, Rb, Cr, Sr and Zn (Table 2).

The Masssadjanga granites are rich in Zr (271 ppm), Cr (180 ppm), Zn (137 ppm), Y (110 ppm), Rb (85 ppm) and Sr (81 ppm). The Karou granites are characterized by their richness in Zr (270 ppm), Cr (180 ppm), Zn (136 ppm), Y (128 ppm), Rb (88 ppm) and Sr (79 ppm).

The Hacker diagrams (Cr, Zr, Sr, Rb and Y) vs $SiO_2$ do not show two groups of

rocks the Karou series and the Massadjanga series. Zr, and Zn, have a profile of almost identical evolution with two negative sloping parts. The Y, Cr and Sr have a only part with negative slope. The Rb presents a part with a positive trend. The behavior of Sr shows its substitution by Ca in plagioclase and alkali feldspar. It is incorporated in apatite and sphenes. That of Rb is incompatible with the fractionation of plagioclase and biotite.

**Table 2.** Chemical composition in Traces elements (% by weight) of representative samples of granite of Iro Lake.

| | A1 | A2 | A3 | A4 | A5 | A6 | Iro 04 | Iro 08 | Iro 09 | Iro 15 | Iro17 | Iro 18 |
|---|---|---|---|---|---|---|---|---|---|---|---|---|
| | ppm | ppm | ppm | ppm | ppm | ppm | ppm | ppm | ppm | ppm | ppm | ppm |
| Be | 77,994 | 60,331 | 56,202 | 70,429 | 3,234 | 82,083 | 5215 | 42,592 | 39,377 | 4.27 | 73,895 | 33,904 |
| V | 17,618 | 21,412 | 264,035 | 26,034 | 1617 | 12,778 | 221,675 | 180,562 | 586,328 | 117,184 | 11,163 | 16,443 |
| Co | 0.9503 | 4732 | 55,294 | 0.7798 | 0.804 | 0.7524 | 45,483 | 36,676 | 12,215 | 36,276 | 0.4133 | 0.7577 |
| Ni | 22,225 | 34,816 | 37,111 | <L.D. | <L.D. | <L.D. | 30,794 | 23,268 | 77,146 | 26,691 | <L.D. | <L.D. |
| Ga | 25,051 | 27,128 | 247,855 | 24,096 | 20.25 | 265,494 | 243,989 | 249,373 | 247,089 | 230,699 | 258,146 | 239,757 |
| Rb | 364.28 | 246.57 | 210,873 | 346.95 | 203.9 | 343,209 | 2,157,064 | 2,478,668 | 1,898,393 | 1,924,955 | 482,636 | 1,793,811 |
| Y | 70,213 | 73,686 | 761,026 | 48.62 | 6934 | 698,744 | 630,338 | 356,017 | 811,671 | 412,318 | 525,499 | 129,356 |
| Nb | 26,042 | 29,383 | 293,275 | 25.86 | 3582 | 265,025 | 24,776 | 211,981 | 447,422 | 165,217 | 332,945 | 4114 |
| Cs | 34,141 | 61,564 | 46,851 | 36,462 | 3.03 | 40,869 | 47,928 | 44,152 | 30,828 | 3656 | 49,103 | 18,966 |
| Ba | 446.11 | 1131.8 | 1137.63 | 438.75 | 1280 | 488,363 | 13,902,897 | 16,932,457 | 1,538,507 | 1,391,537 | 845,779 | 16,505,844 |
| La | 109.23 | 216.85 | 979,624 | 84,613 | 41.64 | 116,293 | 823,331 | 590,259 | 905,845 | 534,101 | 130,007 | 433,197 |
| Ce | 211.01 | 403.13 | 219,672 | 162.05 | 84.62 | 234,716 | 1,892,684 | 1,659,857 | 2,089,072 | 1,049,163 | 295,814 | 738,882 |
| Pr | 22,631 | 42,646 | 262,206 | 17,518 | 6902 | 25,321 | 216,459 | 168,359 | 273,887 | 115,722 | 46,048 | 77,341 |
| Nd | 76,034 | 142.67 | 102,794 | 58,317 | 21.06 | 872,302 | 838,975 | 634,136 | 1,125,345 | 428,618 | 186,996 | 263,991 |
| Sm | 13,297 | 23.18 | 204,172 | 10,409 | 2751 | 160,204 | 170,964 | 123,291 | 229,377 | 7978 | 49,655 | 42,316 |
| Eu | 10,518 | 26,351 | 27,453 | 0.9398 | 2169 | 12,178 | 26,205 | 22,485 | 35,863 | 28,734 | 0.3951 | 30,063 |
| Gd | 10,219 | 17,204 | 16,298 | 80,762 | 1892 | 123,397 | 133,882 | 89,688 | 18,228 | 67,564 | 50,372 | 31,197 |
| Dy | 9893 | 14,101 | 143,615 | 78,815 | 136 | 113,005 | 118,705 | 76,697 | 157,733 | 64,229 | 66,078 | 24,027 |
| Ho | 2173 | 27,518 | 28,448 | 16,699 | 0.266 | 23,394 | 23,517 | 1455 | 31,031 | 14,089 | 15,944 | 0.4784 |
| Er | 64,421 | 73,781 | 76,652 | 49,335 | 0.745 | 68,004 | 62,846 | 38,676 | 8.18 | 40,709 | 52,545 | 13,345 |
| Tm | 0.9852 | 10,351 | 10,647 | 0.769 | 0.116 | 10,537 | 0.8838 | 0.5486 | 11,292 | 0.6062 | 0.9659 | 0.1999 |
| Yb | 69,776 | 69,743 | 71,714 | 5.74 | 0.854 | 7711 | 6081 | 38,375 | 76,325 | 43,011 | 80,145 | 14,312 |
| Lu | 10,563 | 10,052 | 10,579 | 0.859 | 0.137 | 11,499 | 0.877 | 0.5639 | 11,236 | 0.6814 | 13,861 | 0.2195 |
| Hf | 72,906 | 14,104 | 139,994 | 77,145 | 2577 | 86,747 | 120,977 | 105,571 | 170,725 | 96,431 | 67,338 | 2095 |

**Continued**

| | | | | | | | | | | | | |
|---|---|---|---|---|---|---|---|---|---|---|---|---|
| Ta | 29,723 | 25,684 | 24,411 | 31,428 | 0.412 | 32,963 | 20,228 | 17,813 | 28,069 | 13,254 | 25,976 | 0.4757 |
| W | 0.8748 | 0.907 | 10,979 | 0.9482 | <L.D. | 10,663 | 13,713 | 17,171 | 11,481 | 13,056 | 1615 | <L.D. |
| Th | 49,929 | 34,499 | 179,002 | 56,454 | 16.49 | 547,851 | 126,366 | 9906 | 73,969 | 84,117 | 301,078 | 97,892 |
| U | 89,963 | 45,643 | 47,139 | 12.94 | 1728 | 84,376 | 2327 | 26,579 | 27,621 | 18,705 | 284,103 | 2576 |
| Cr | 40,824 | 58,817 | 67,025 | 3319 | 2503 | 3447 | 4717 | 42,315 | 216,372 | 92,512 | 2967 | 29,432 |

Normalization of trace elements

The trace elements of the Massadjanga granites are standardized to the Primitive Mantle considered magma source in the logarithmic diagram.

Rare earths

Massadjanga granites

In the rock/primitive mantle diagram, the alkaline granites present a spectrum of rare earths marked by a positive anomaly in Yb, and a negative anomaly in Eu and an appearance decreasing from La to Sm and from Gd to Lu.

The rare earth spectra of the Massadjanga granites show a sloping appearance decreasing from light rare earths to heavy rare earths via intermediaries. They present negative anomalies in Europium (Eu) and one positive anomaly in Ytterbium (Yb) (Figure 11).

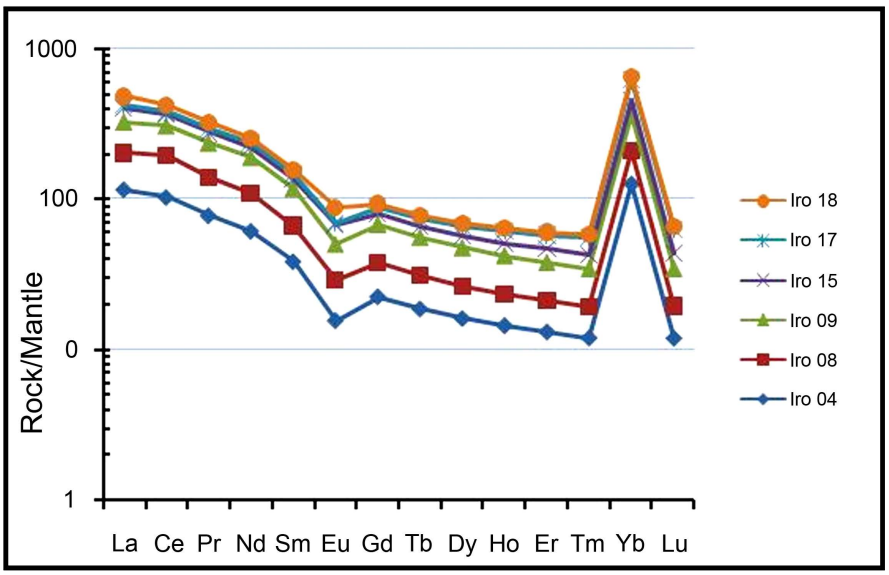


Figure 11. Rare Earth spectra of Massadjanga granite from the Lake Iro massif. Normalization against the Primitive Mantle of [34].

The Massadjanga granites present a profile reflecting a rate of fractionation weak. The sum of the rare earth contents of these rocks is (REE = 156 ppm). Quite different by their rare earth content, these rocks present a small negative anomaly in Eu which is confirmed by the ratio [Eu/Eu* = EuN/((SmN) × (GdN)) 1/2],

Eu/Eu* = 0.484 ppm. This brings us to consider that the evolution between these rocks would be controlled by the fractionation of zircon, apatite, sphene and plagioclase. The ratio (Sm/Nd)N = 0.881 ppm is less than unity while that of (La/Lu)N = 2.16 is greater than unity.

Rock normalization to MORB

The Massadjanga granites display spectra marked by positive anomalies in $K_2O$, Rb, Ba, Th, La, Ce, Sm, Hf, y and Yb, and negative anomalies in Sr, Nb, $P_2O_5$ and $TiO_2$ (**Figure 12**).

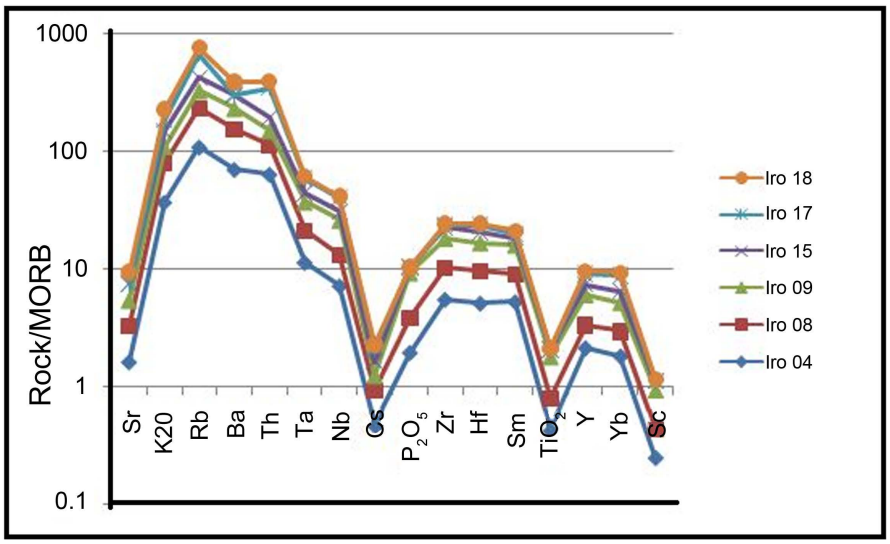


**Figure 12.** Spidergram of the Massadjanga granites of the Lac Iro massif normalized in relation [35] Sc and Cr from [35].

The positive anomaly in $K_2O$, Rb and Ba reflects the enrichment of biotite granites in these elements. The negative anomaly in $P_2O_5$ shows the fractionation of apatite and that of $TiO_2$ reveals the fractionation of ferrotitanium oxides ($TiO_2$).

The positive anomaly in Rb suggests substitution potassium in alkali feldspar. The slight positive anomaly in Zr highlights the possible substitution of Zr, Ti in accessory minerals such as zircon.

The positive Yb anomaly reflects the enrichment of the rocks in zircon.

Negative anomalies in (Sr, Nb, $P_2O_5$ and $TiO_2$) and positive in ($K_2O$, Rb and Ba) show that granitoids have for the source the continental crust. The negative anomaly in Ta and $TiO_2$ shows that the granites of Massadjanga were set up in a subduction environment.

Karou granites

In the rock/primitive mantle diagram, the alkaline granites present a spectrum of rare earths marked by a positive anomaly in Yb, and a negative anomaly in Eu and an appearance decreasing from La to Sm and Gd to Tm.

(**Figure 13**) Rare Earth spectra of Karou granite from the Lake Iro massif normalized by relation to the Primitive Mantle of [34].

The rare earth spectra of the Karou granites show a sloping appearance decreas-

ing from light rare earths to heavy rare earths via intermediaries. They present negative anomalies in Europium (Eu) and one positive anomaly in Ytterbium Yb.

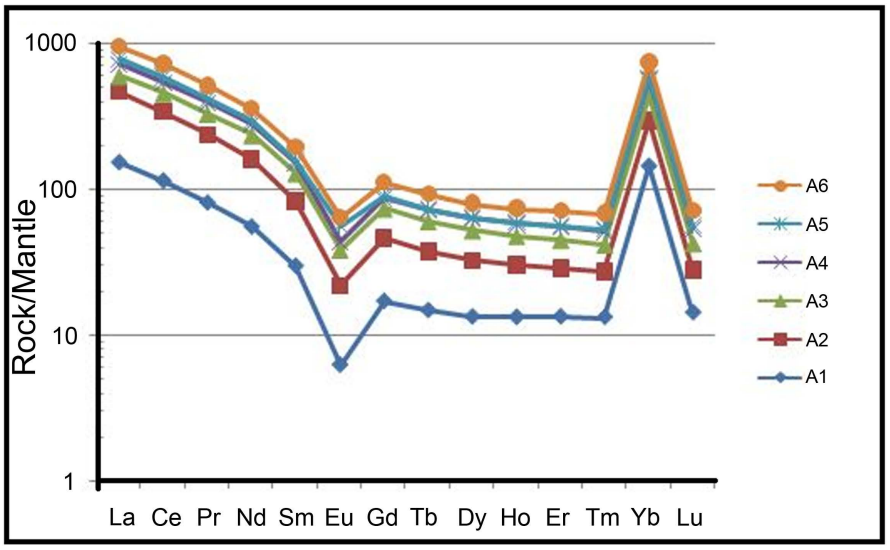


**Figure 13.** Rare Earth spectra of Karou granite from the Iro Lake massif normalized to the primitive mantle of [34].

The Karou granites have a profile reflecting a low fractionation rate. The sums of rare earth contents of these rocks are respectively (REE = 156 and 239 ppm).

These rocks present a negative anomaly in Eu which is confirmed by the ratio [Eu/Eu* = EuN/((SmN) × (GdN)) 1/2], Eu/Eu* = 0.484 ppm and a positive Yb anomaly. This brings us to consider that the evolution between these rocks would be controlled by the fractionation of zircon, apatite, sphene and plagioclase.

Rare Earth profile shows weak fractionation in the Karou granites: (La/Yb)N = 2.13. In this profile, we note that the Karou granites have a ratio (Gd/Yb)N = 1.123, this value greater than unity suggests that these rocks are highly fractionated. The ratio (Sm/Nd)N = 0.881 is less than unity while that of (La/Lu)N = 2.16 is greater than unity.

Normalization of phased arrays

Rock normalization to MORB

The Karou granites display spectra showing positive Rb anomalies, and Th, and negative anomalies in Ba, Cs, $P_2O_5$, $TiO_2$ and Sc (**Figure 14**).

Normalization of phased arrays

The positive anomaly in Rb and Th reflects the enrichment of the Karou granites in these elements. The negative anomaly in Cs shows the fractionation of apatite and that of $TiO_2$ reveals the fractionation of ferrotitanium oxides.

The positive anomaly in Rb suggests the substitution of potassium in the alkali feldspar. The slight positive anomaly in Th highlights the possible substitution of Th and Ba in accessory minerals such as zircon. Negative anomalies in Ba, Cs, $P_2O_5$, $TiO_2$ and Sc and positive in Rb and Th show that granitoids have a source in the continental crust. The negative anomaly in Cs and $TiO_2$ shows

that the Karou granites were emplaced in a subduction environment. According to [36], the $TiO_2$ contents >0.20 characteristic is indicative of his non-mantelic origin.

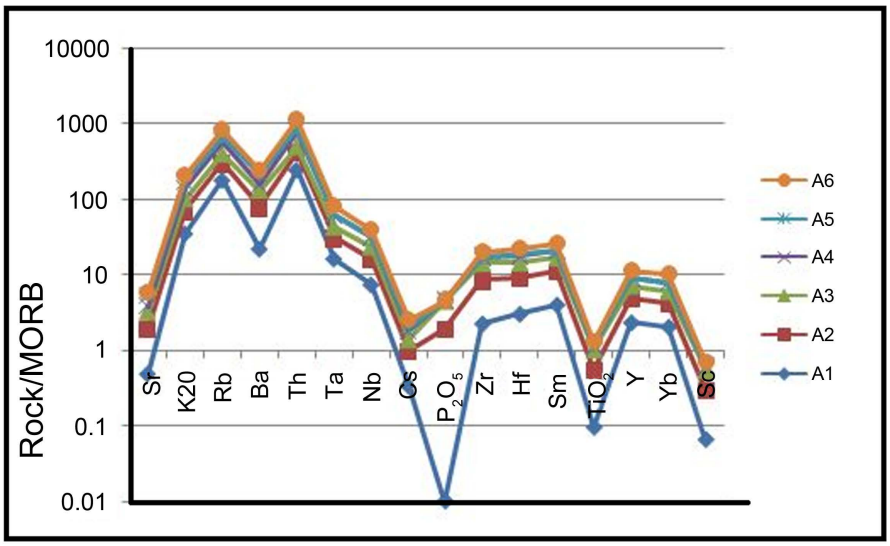


**Figure 14.** Spidergram of the Karou granites of the Lac Iro massif normalized in relation to [35] Sc and Cr from [35].

## 5. Discussion

Granitoids in the studied area are granites with basic enclaves. The enclaves also reflect incomplete mixing, a low proportion of injected basic material and poor representation in the plutonic rock [37]. According to the work of [38]-[41], the disintegration of dykes in host magmas influenced by the rheology of the materials involved is also at the origin of enclaves.

The Lake Iro granitoids have relatively high A/CNK and $K_2O/Na_2O$ ratios which are compatible with a type S affinity indicating the presence of peraluminous minerals (example of muscovite). Where S-type granites are defined as being strongly peraluminous, with $Al_2O_3/(CaO + Na_2O + K_2O) > 1.1$ [42]. This is mainly due to their low Na and Ca, which are interpreted to be lost to solution during weathering, unlike K, which is preferentially sequestered by clays during this process, raising K/Na [43]. Additionally, S-type granites are generally thought to form magmas generated by partial melting underwater under-saturation conditions [44]. The geochemical study shows that the granitoids in the studied area are granites containing biotite, aplites and pegmatites having a source coming from partial fusion. The belonging to a magmatic source of these granites is confirmed by the evolution geochemistry of major and trace elements in Hacker diagrams. The role of plagioclase fractionation was relatively major during the earlier intrusive stages (consistent with the presence of Eu anomalies) and slightly increased, together with biotite and K-feldspar fractionation, during the later (granitic) rock crystallization.

The negative anomalies in Eu and Cr observed show the importance of the frac-

tionation of feldspars during their genesis. This type of environment is characteristic of subduction zones. This discussion is in agreement with the regional geodynamic framework which considers that the block is an ancient active margin [11] [24] [29]. The igneous rocks of Lake Iro are characterized by their iron mineralogy, define a ferric metalliferous-calcium metaluminous to weakly peraluminous potassium association and have high HFSE (Nb, Y) and REE contents. In addition, S-type granites are generally thought to form from magmas generated by the partial melting of metapelite and metagraywacke material in underwater-undersaturated conditions [45]-[47]. Therefore, they are better classified as S-type granites and are variably ferromagnetic. The Lake Iro granites correspond to a single subvolcanic-silicic complex plutonic because first-order geochemical modeling indicates that microgranites can be generated by fractional crystallization of an assembly of two feldspars-amphiboles from a molten porphyry granite. Then, the granites of Iro Lake represent the oldest in a series of post-collisional igneous associations exposed in southern Chad and neighboring countries which, collectively, show that the amalgamation of the blocs constituent parts of the South-Saharan meta craton is older than 580 Ma [11] [24] [29].

The South, Southeast region of Chad is located in a critical domain at the southern margin of the Saharan Meta-craton and inside what we call the Oubanguides or Central African orogenic belts which connect it to the Congo craton [18] [48] [49].

## 6. Conclusions

This work focused on the petrography and geochemistry of granitoids in the North-West sector of the department of Iro Lake, one of the objectives is to map the formations of the Precambrian age in southeastern Chad. At the end of this study, the results are grouped around two major subjects: petrography and geochemistry. The lithological study area is composed of igneous and sedimentary rocks. Magmatic rocks constitute the most abundant and varied types of granitoids. They are represented by the biotite granites and leucogranites with which vein rocks are associated (aplites, pegmatites) and basic enclaves. The mineralogical assemblage is made up of quartz + plagioclase + alkaline feldspar + biotite. Field observations show a clear magmatic differentiation marked by different facies observed on the same outcrop (porphyry granites, dark and light fine-grained granites, enclaves).

On the geochemical analysis, the results show that the granitoids are subalkaline to calc-alkaline with high K content. Granitoids are identified as peraluminous granites with type S. The geodynamic context is that of a subduction zone.

The REEs normalized to the primitive mantle reflecting the crystallization process and the fractional crystallization of plagioclase. The role of plagioclase fractionation was relatively major during the earlier intrusive stages (consistent with the presence of Eu anomalies) and slightly increased, together with biotite and K-feldspar fractionation, during the later (granitic) rock crystallization. Normaliza-

tion of multielement to MORBs indicates losses of Ba, Ti and Cs which can be caused by the fractionation of plagioclase, apatite and ilmenite. The Ba anomaly is also controlled by the presence of K-feldspar and mica. The observed Ti anomalies are due to the fractionation of magnetite indicating a subduction environment (or remelting of a source from a subduction environment).

## Acknowledgements

The authors are great to GELT project for supporting the field work.

## Conflicts of Interest

The authors declare no conflicts of interest regarding the publication of this paper.

## References

[1] Goodge, J.W. and Vervoort, J.D. (2006) Origin of Mesoproterozoic A-Type Granites in Laurentia: Hf Isotope Evidence. *Earth and Planetary Science Letters*, **243**, 711-731. https://doi.org/10.1016/j.epsl.2006.01.040

[2] Kemp, A.I.S. and Hawkesworth, C.J. (2003) Granitic Perspectives on the Generation and Secular Evolution of the Continental Crust. *Treatise on Geochemistry*, **3**, 349-410. https://doi.org/10.1016/b0-08-043751-6/03027-9

[3] Heilimo, E., Elburg, M.A. and Andersen, T. (2014) Crustal Growth and Reworking during Lapland-Kola Orogeny in Northern Fennoscandia: U-Pb and Lu-Hf Data from the Nattanen and Litsa-Aragub-Type Granites. *Lithos*, **205**, 112-126. https://doi.org/10.1016/j.lithos.2014.06.014

[4] Taylor, S.R. and McLennan, S.M. (1985) The Continental Crust: Its Composition and Evolution. Blackwell Scientific Publications.

[5] Hawkesworth, C.J., Dhuime, B., Pietranik, A.B., Cawood, P.A., Kemp, A.I.S. and Storey, C.D. (2010) The Generation and Evolution of the Continental Crust. *Journal of the Geological Society*, **167**, 229-248. https://doi.org/10.1144/0016-76492009-072

[6] White, A.J.R. and Chappell, B.W. (1983) Granitoid Types and Their Distribution in the Lachlan Fold Belt, Southeastern Australia. In: Roddick, J.A., Ed., *Geological Society of America Memoirs*, Geological Society of America, 21-34. https://doi.org/10.1130/mem159-p21

[7] Chappell, B.W. and White, A.J.R. (1992) I- and S-Type Granites in the Lachlan Fold Belt. *Earth and Environmental Science Transactions of the Royal Society of Edinburgh*, **83**, 1-26. https://doi.org/10.1017/s0263593300007720

[8] Champion, D.C. and Chappell, B.W. (1992) Petrogenesis of Felsic I-Type Granites: An Example from Northern Queensland. *Earth and Environmental Science Transactions of the Royal Society of Edinburgh*, **83**, 115-126. https://doi.org/10.1017/s026359330000780x

[9] Chappell, B.W. and White, A.J.R. (1974) Two Contrasting Granite Types. *Pacific Geology*, **8**, 173-174.

[10] Bouyo Houketchang, M., Toteu, S.F., Deloule, E., Penaye, J. and Van Schmus, W.R. (2009) U-Pb and Sm-Nd Dating of High-Pressure Granulites from Tcholliré and Banyo Regions: Evidence for a Pan-African Granulite Facies Metamorphism in North-Central Cameroon. *Journal of African Earth Sciences*, **54**, 144-154. https://doi.org/10.1016/j.jafrearsci.2009.03.013

[11] Couzinié, S., Ménot, R., Doumnang, J., Paquette, J., Rochette, P., Quesnel, Y., *et al*.

(2020) Crystalline Inliers Near Lake Iro (SE Chad): Post-Collisional Ediacaran A2-Type Granitic Magmatism at the Southern Margin of the Saharan Metacraton. *Journal of African Earth Sciences*, **172**, Article ID: 103960. https://doi.org/10.1016/j.jafrearsci.2020.103960

[12] Reimold, W.U. and Koeberl, C. (2014) Impact Structures in Africa: A Review. *Journal of African Earth Sciences*, **93**, 57-175. https://doi.org/10.1016/j.jafrearsci.2014.01.008

[13] Poulin, C., Hamelin, B., Vallet-Coulomb, C., Amngar, G., Loukman, B., Cretaux, J., *et al*. (2019) Unraveling the Hydrological Budget of Isolated and Seasonally Contrasted Subtropical Lakes. *Hydrology and Earth System Sciences*, **23**, 1705-1724. https://doi.org/10.5194/hess-23-1705-2019

[14] Bessole, B. and Trompette, R. (1980) La chaine panafricaine zone mobile d'Afrique Centrale et zone mobile soudanaise. Géologie Afrique, mÉmoire BRGM Orléans (France) 2, 397.

[15] Castaing, C., Feybesse, J.L., Thiéblemont, D., Triboulet, C. and Chèvremont, P. (1994) Palaeogeographical Reconstructions of the Pan-African/brasiliano Orogen: Closure of an Oceanic Domain or Intracontinental Convergence between Major Blocks? *Precambrian Research*, **69**, 327-344. https://doi.org/10.1016/0301-9268(94)90095-7

[16] Black, M. and Kasse, Y. (1995) Mission géologique au Tchad. Rapport de mission BRGM-PNUD (Rapport inédit).

[17] Liégeois, J.P., Latouche, L., Navez, J. and Black, R. (1994) Earth and Late Pan-African Orogenies in the Tuareg Shield: Relations with East Saharan Ghost Craton and the West African Craton. *Journal of African Earth Sciences*, **30**, 53-54.

[18] Toteu, S.F., Penaye, J. and Djomani, Y.P. (2004) Geodynamic Evolution of the Pan-African Belt in Central Africa with Special Reference to Cameroon. *Canadian Journal of Earth Sciences*, **41**, 73-85. https://doi.org/10.1139/e03-079

[19] Ngako, V. (1999) Les déformations continentales panafricaines en Afrique Centrale. Résultats d'un poinçonnement de type himalayen. Master's Thesis, Université de Yaoundé I.

[20] Ferré, E., Gleizes, G. and Caby, R. (2002) Obliquely Convergent Tectonics and Granite Emplacement in the Trans-Saharan Belt of Eastern Nigeria: A Synthesis. *Precambrian Research*, **114**, 199-219. https://doi.org/10.1016/s0301-9268(01)00226-1

[21] Schneider, J.L. and Wolff, J.P. (1992) Carte géologique et cartes Hydrogéologiques à 1/1.500.000 de la République du Tchad: Mémoire explicatif. Bureau de Recherches Géologiques et Minières.

[22] Maurin, J. and Guiraud, R. (1993) Basement Control in the Development of the Early Cretaceous West and Central African Rift System. *Tectonophysics*, **228**, 81-95. https://doi.org/10.1016/0040-1951(93)90215-6

[23] Shellnutt, J.G., Lee, T.Y., Torng, P.K., Yang, C.C. and Lee, Y.H. (2016) Late Cretaceous Intraplate Silicic Volcanic Rocks from the Lake Chad Region: An Extension of the Cameroon Volcanic Line? *Geochemistry, Geophysics, Geosystems*, **17**, 2803-2824. https://doi.org/10.1002/2016gc006298

[24] Pouclet, A., Vidal, M., Doumnang, J.-C., Vicat, J.-P. and Tchameni, R. (2006) Neoproterozoic Crustal Evolution in Southern Chad: Pan-African Ocean Basin Closing, Arc Accretion and Late- to Post-Orogenic Granitic Intrusion. *Journal of African Earth Sciences*, **44**, 543-560. https://doi.org/10.1016/j.jafrearsci.2005.11.019

[25] Schneider, J. and Wolff, J. (1992) Carte géologique et cartes hydrogéologiques à 1/1 500 000 de la République du Tchad. Mémoire explicatif [Geological Map and Hydro-

geological Maps at 1/1,500,000 of the Republic of Chad. Explanatory Memorandum]. Memoire Explicatif. Documents du BRGM no 209, Orleans (France), 443.

[26] Kusnir, I. (1995) Géologie, ressources minérales et ressources en eau du Tchad; Travaux et documents scientifiques du Tchad, connaissance du Tchad. Centre National de Recherche, 115.

[27] Gsell, J. and Sonnet, J. (1960) Carte géologique de reconnaissance au 1/500.000 et notice explicative sur la feuille Adre. Brazzaville. BRGM, 42.

[28] Pias, J. and Barbery, J. (1965) Cartes pédologiques de reconnaissance au 1:200 000, feuille de lac Iro-Djouna. République du Tchad, 106.

[29] Doumnang, J.C. (2006) Géologie des formations néoprotérozoïques du Mayo-Kebbi (Sud-ouest du Tchad): Apports de la pétrologie et de la géochimie, implications sur la géodynamique au Panafricain. Université d'Orléans, 86-117.

[30] Irvine, T.N. and Baragar, W.R.A. (1971) A Guide to the Chemical Classification of the Common Volcanic Rocks. *Canadian Journal of Earth Sciences*, **8**, 523-548. https://doi.org/10.1139/e71-055

[31] Le Maitre *et al*. (1989) Download Scientific Diagram/Diagramme $SiO_2$ vs $Na_2O+K_2O$ appliqué aux roches magmatiques du Group de Ouarzazate (NP3sW).

[32] Rickwood, P.C. (1989) Boundary Lines within Petrologic Diagrams Which Use Oxides of Major and Minor Elements. *Lithos*, **22**, 247-263. https://doi.org/10.1016/0024-4937(89)90028-5

[33] Barbarin, B. (1996) Genesis of the Two Main Types of Peraluminous Granitoids. *Geology*, **24**, 295-298. https://doi.org/10.1130/0091-7613(1996)024<0295:gottmt>2.3.co;2

[34] Mandler, J.M., Bauer, P.J. and McDonough, L. (1991) Separating the Sheep from the Goats: Differentiating Global Categories. *Cognitive Psychology*, **23**, 263-298. https://doi.org/10.1016/0010-0285(91)90011-c

[35] Pearce, J.A. (1983) Role of the Sub-Continental Lithosphere in Magma Genesis at Active Continental Margins. In: Hawkesworth, C.J. and Norry, M.J., Eds., *Continental Basalts and Mantle Xenoliths*, Shiva Cheshire, 230-249.

[36] Kamenetsky, V.S. (2001) Factors Controlling Chemistry of Magmatic Spinel: An Empirical Study of Associated Olivine, Cr-Spinel and Melt Inclusions from Primitive Rocks. *Journal of Petrology*, **42**, 655-671. https://doi.org/10.1093/petrology/42.4.655

[37] Barbarin, B. (1990) Granitoids: Main Petrogenetic Classifications in Relation to Origin and Tectonic Setting. *Geological Journal*, **25**, 227-238. https://doi.org/10.1002/gj.3350250306

[38] Barbarin, B. (2005) Mafic Magmatic Enclaves and Mafic Rocks Associated with Some Granitoids of the Central Sierra Nevada Batholith, California: Nature, Origin, and Relations with the Hosts. *Lithos*, **80**, 155-177. https://doi.org/10.1016/j.lithos.2004.05.010

[39] Barbarin, B. and Didier, J. (1992) Genesis and Evolution of Mafic Microgranular Enclaves through Various Types of Interaction between Coexisting Felsic and Mafic Magmas. *Earth and Environmental Science Transactions of the Royal Society of Edinburgh*, **83**, 145-153. https://doi.org/10.1017/s0263593300007835

[40] Castro, A., de la Rosa, J.D. and Stephens, W.E. (1990) Magma Mixing in the Subvolcanic Environment: Petrology of the Gerena Interaction Zone near Seville, Spain. *Contributions to Mineralogy and Petrology*, **106**, 9-26. https://doi.org/10.1007/bf00306405

[41] Turnbull, R., Weaver, S., Tulloch, A., Cole, J., Handler, M. and Ireland, T. (2010)

Field and Geochemical Constraints on Mafic-Felsic Interactions, and Processes in High-Level Arc Magma Chambers: An Example from the Halfmoon Pluton, New Zealand. *Journal of Petrology*, **51**, 1477-1505. https://doi.org/10.1093/petrology/egq026

[42] Chappell, B.W. and White, A.J.R. (2001) Two Contrasting Granite Types: 25 Years Later. *Australian Journal of Earth Sciences*, **48**, 489-499. https://doi.org/10.1046/j.1440-0952.2001.00882.x

[43] Nesbitt, H.W., Markovics, G. and price, R.C. (1980) Chemical Processes Affecting Alkalis and Alkaline Earths during Continental Weathering. *Geochimica et Cosmochimica Acta*, **44**, 1659-1666. https://doi.org/10.1016/0016-7037(80)90218-5

[44] Li, J., Qian, Y., Tekoumc, L., Zhao, C., Sun, J., Zheng, T., *et al*. (2021) Petrogenesis of Jurassic Granitoids on Liaodong Peninsula, Northeast China: Constraints on the Evolution of the Mongol-Okhotsk and Pacific Tectonic Regimes. *Journal of Earth Science*, **32**, 127-143. https://doi.org/10.1007/s12583-020-1372-0

[45] Guo, Z. and Wilson, M. (2012) The Himalayan Leucogranites: Constraints on the Nature of Their Crustal Source Region and Geodynamic Setting. *Gondwana Research*, **22**, 360-376. https://doi.org/10.1016/j.gr.2011.07.027

[46] Harris, N.B.W., Pearce, J.A. and Tindle, A.G. (1986) Geochemical Characteristics of Collision-Zone Magmatism. *Geological Society*, *London*, *Special Publications*, **19**, 67-81. https://doi.org/10.1144/gsl.sp.1986.019.01.04

[47] Abdelsalam, M.G., Liégeois, J. and Stern, R.J. (2002) The Saharan Metacraton. *Journal of African Earth Sciences*, **34**, 119-136. https://doi.org/10.1016/s0899-5362(02)00013-1

[48] Patino Douce, A.E. and Harris, N. (1998) Experimental Constraints on Himalayan Anatexis. *Journal of Petrology*, **39**, 689-710. https://doi.org/10.1093/petroj/39.4.689

[49] Pin, C. and Poidevin, J. (1987) U-pb Zircon Evidence for a Pan-African Granulite Facies Metamorphism in the Central African Republic. a New Interpretation of the High-Grade Series of the Northern Border of the Congo Craton. *Precambrian Research*, **36**, 303-312. https://doi.org/10.1016/0301-9268(87)90027-1